Amphiphilic proteins coassemble into multiphasic condensates and act as biomolecular surfactants

Fleurie M. Kelley[a,1], Bruna Favetta[b,1], Roshan Mammen Regy[c], Jeetain Mittal[c], and Benjamin S. Schuster[a,2]

[a]Department of Chemical and Biochemical Engineering, Rutgers, the State University of New Jersey, Piscataway, NJ 08854; [b]Department of Biomedical Engineering, Rutgers, the State University of New Jersey, Piscataway, NJ 08854; and [c]Artie McFerrin Department of Chemical Engineering, Texas A&M University, College Station, TX 77843

Edited by Michael Rosen, Department of Biophysics, The University of Texas Southwestern Medical Center, Dallas, TX; received May 28, 2021; accepted November 3, 2021

Cells contain membraneless compartments that assemble due to liquid–liquid phase separation, including biomolecular condensates with complex morphologies. For instance, certain condensates are surrounded by a film of distinct composition, such as Ape1 condensates coated by a layer of Atg19, required for selective autophagy in yeast. Other condensates are multiphasic, with nested liquid phases of distinct compositions and functions, such as in the case of ribosome biogenesis in the nucleolus. The size and structure of such condensates must be regulated for proper biological function. We leveraged a bioinspired approach to discover how amphiphilic, surfactant-like proteins may contribute to the structure and size regulation of biomolecular condensates. We designed and examined families of amphiphilic proteins comprising one phase-separating domain and one non–phase-separating domain. In particular, these proteins contain the soluble structured domain glutathione S-transferase (GST) or maltose binding protein (MBP), fused to the intrinsically disordered RGG domain from P granule protein LAF-1. When one amphiphilic protein is mixed in vitro with RGG-RGG, the proteins assemble into enveloped condensates, with RGG-RGG at the core and the amphiphilic protein forming the surface film layer. Importantly, we found that MBP-based amphiphiles are surfactants and influence droplet size, with increasing surfactant concentration resulting in smaller droplet radii. In contrast, GST-based amphiphiles at increased concentrations coassemble with RGG-RGG into multiphasic structures. We propose a mechanism for these experimental observations, supported by molecular simulations of a minimalist model. We speculate that surfactant proteins may play a significant role in regulating the structure and function of biomolecular condensates.

liquid–liquid phase separation | surfactants | size regulation | intrinsically disordered proteins | molecular simulations

The intracellular environment is like a complex emulsion. This paradigm originated more than a century ago but is enjoying a renaissance, with recent discoveries revealing the important role of liquid–liquid phase separation (LLPS) in biology (1–3). LLPS of proteins and nucleic acids underlies the formation of membraneless organelles, alternatively called biomolecular condensates, which are distinct intracellular compartments that lack a delimiting membrane (2, 3). Biomolecular condensates contribute to numerous cell functions, including stress response, gene regulation, and signaling (4). Conversely, aberrant phase separation due to mutations and age-related processes is implicated in diseases such as neurodegeneration and cancer (5). Deciphering the rules of self-assembly of biomolecular condensates has therefore emerged as a promising avenue for elucidating fundamental principles of biological structure, function, and dysfunction.

Despite significant recent progress in understanding the biophysics of biomolecular condensates, many open questions remain (6). One key question is what molecular phenomena govern the spontaneous assembly of condensates with core-shell or multiphasic structures. Another important question is how cells tune the size of biomolecular condensates. Here, we sought to gain insight into both questions by examining how amphiphilic, surfactant-like proteins contribute to the self-assembly and regulation of biomolecular condensates. Amphiphiles are typically defined as molecules comprising separate hydrophilic and hydrophobic parts. Here, we note the etymology (in Greek, "amphi" means both, and "philia" means friendship or love) and use the term amphiphile to describe proteins comprising one domain that has affinity for biomolecular condensates and one domain that has affinity for the dilute phase.

Surfactants are substances, generally amphiphiles, that adsorb to interfaces and decrease interfacial tension. Extracellularly, pulmonary surfactant lining the alveoli plays a vital role in lung physiology by reducing the work of breathing (7, 8). However, the role of surfactants in the emulsion-like intracellular milieu is just beginning to be explored (9). In biological systems, the surfactant-like protein Ki-67 prevents individual chromosomes from coalescing during early stages of mitosis by forming a repulsive molecular brush layer (10). Some biomolecular condensates are reminiscent of surfactant-laden emulsions, although their physical chemistry remains to be elucidated. For instance, Atg19 forms a thin surface layer surrounding Ape1 condensates that is necessary for selective autophagy of Ape1 in yeast (11). Inspired by such examples, we hypothesized that a minimal system

Significance

Membraneless organelles are assemblies of highly concentrated biomolecules that condense through liquid–liquid phase separation. One major question in the field is how proteins assemble into multilayered condensates. Understanding mechanisms of formation of these systems is important for understanding the function and regulation of multiphasic organelles, such as P granules and nucleoli. A second outstanding question is how the size of biomolecular condensates is controlled. In this work, we generated amphiphilic proteins that localize to the surface of condensates. We observed diverse assemblies, including condensates enveloped by surfactant-like films, as well as complex multiphasic morphologies. In some configurations, these surfactant-like proteins influence condensate size. Our results suggest an important role of protein amphiphiles in establishing membraneless organelle structure and function.

Author contributions: F.M.K., B.F., R.M.R., J.M., and B.S.S. designed research; F.M.K., B.F., R.M.R., and B.S.S. performed research; F.M.K., B.F., R.M.R., and B.S.S. analyzed data; and F.M.K., B.F., R.M.R., J.M., and B.S.S. wrote the paper.

The authors declare no competing interest.

This article is a PNAS Direct Submission.

[1]F.M.K. and B.F. contributed equally to this work.

[2]To whom correspondence may be addressed. Email: bss142@soe.rutgers.edu.

This article contains supporting information online at http://www.pnas.org/lookup/suppl/doi:10.1073/pnas.2109967118/-/DCSupplemental.

Published December 16, 2021.

comprising surfactant-like proteins interacting with phase-separating proteins could recapitulate enveloped condensate structures observed in nature.

Moreover, condensates exhibit a variety of multiphase and multilayer structures underpinning their biological functions. Bre1 assembles as a shell surrounding Lge1 condensates, generating a catalytic condensate that functions to accelerate ubiquitination of histone H2B in yeast (12). The nucleolus is comprised of coexisting liquid phases of differing interfacial tensions (13), while P granules contain coexisting liquid and gel phases (14). Stress granules (15), nuclear speckles (16), paraspeckles (17), and reconstituted polypeptide/RNA complex coacervates also exhibit core-shell structures sensitive to stoichiometry and competitive binding (18–21). Functionally related condensates can remain in contact without coalescing, as in the case of stress granules and P-bodies (22) or P granules and Z granules (23). We asked whether amphiphilic proteins could contribute to the complex morphologies of biomolecular condensates that have been observed within cells, just as synthetic amphiphiles and surfactant systems exhibit rich structures and phase behaviors (24).

Surfactant-like proteins could have additional important functional consequences, including but not limited to modulating biomolecular condensate size, which in turn influences biochemical processes through condensate size-dependent effects on molecular concentrations and diffusion (25, 26). Biomolecular condensates are often observed in cells as multiple smaller droplets rather than as a single larger droplet, even though the latter is expected to be thermodynamically favored. Recent studies have attributed the apparent metastability of biomolecular condensates in various contexts to surface charge (27), cytoskeletal caging (28, 29), membrane association (30), and exhaustion of available binding sites (31). Active processes can also maintain the emulsified, multidroplet state in vivo (32). An additional possibility, which we examine here, is that surfactant proteins may help stabilize biomolecular condensates.

To address these questions, we adopted a bottom-up, bioinspired approach, seeking to leverage a simplified system to shed light on the role of amphiphilic proteins in the self-assembly of biomolecular condensates. We designed amphiphilic proteins containing an intrinsically disordered region (IDR) fused to folded domains. The IDR is a phase-separating domain, whereas the folded domains alone are not. When one of these amphiphilic fusion proteins is mixed at low concentrations with the IDR, the two proteins assemble such that the amphiphilic protein forms a film that coats the IDR core. We demonstrate several extensions of this observation, including the important finding that condensate size can be influenced by varying surfactant protein concentration. Furthermore, when amphiphilic proteins with different folded domains are mixed together with the core IDR, we observe competition between different surfactant proteins for binding to the condensate interface. Interestingly, one family of amphiphilic proteins exhibits varied morphologies, including multiphasic condensates, and we map the rich, concentration-dependent phase behavior. To gain mechanistic insight into these experimental observations, we present a minimalistic computational model that recapitulates the range of behaviors observed experimentally by varying the strength of interaction between domains. Our experiments and simulations suggest that amphiphile–condensate assembly is determined by the strength of interaction between the amphiphile and the IDR core as well as interactions between the folded domain of the amphiphile. Taken together, this work illustrates the diverse interfacial phenomena that can arise from interactions between condensates and amphiphilic proteins, notably raising the possibility that surfactant proteins may play a significant role in regulating the structure and function of biomolecular condensates.

Results

Designing Amphiphilic Proteins to Act as Biological Surfactants. In prior work, we examined the partitioning of client proteins into biomolecular condensates (33). We focused on the RGG domain from LAF-1, a prototypical arginine/glycine-rich intrinsically disordered protein (IDP) involved in P granule assembly in *Caenorhabditis elegans* (34–36). Tandem repeats of the RGG domain (RGG-RGG) phase-separate in vitro at concentrations >1 μM under physiological conditions. We found that RFP and GST-RFP are mostly excluded from RGG-RGG condensates; RFP denotes red fluorescent protein and GST denotes glutathione S-transferase, which is widely used as a solubility-enhancing affinity tag in recombinant protein production (37). In contrast, we observed that RFP fused to one or two RGG domains partitioned into RGG-RGG condensates. These results demonstrated that client partitioning into or exclusion from RGG-RGG condensates depends on the balance between the "RGG-philic" and "RGG-phobic" content of the client protein. Here, we hypothesized that a third, intermediate outcome is possible: that with the right balance, a client protein may localize to the interface between the condensate and dilute phases, coating the condensate and displaying surfactant-like behavior.

We therefore asked whether we could engineer amphiphilic proteins that assemble as a film on the surface of RGG-RGG condensates. We designed a family of amphiphilic fusion proteins containing a phase-separating domain (RGG-philic) fused to a non-phase-separating domain (RGG-phobic) (*SI Appendix*, Fig. S1). Two representative protein constructs from this family are MBP-GFP-RGG and GST-GFP-RGG (Fig. 1*A*). MBP denotes maltose binding protein, which, like GST, is a well-known affinity tag that enhances protein solubility (37–40). GFP denotes enhanced green fluorescent protein with the monomerizing A206K mutation. By combining RGG, GST, MBP, and fluorescent protein domains, our aim was to generate amphiphilic fusion proteins with RGG-philic and RGG-phobic parts. We hypothesized that upon mixing the amphiphilic proteins with RGG-RGG, the poorly soluble RGG domain in the amphiphiles would interact with and orient toward the inner RGG-RGG condensate phase, while the RGG-phobic MBP and GST domains would interact with and orient toward the outer dilute phase (Fig. 1*B*).

Amphiphilic Proteins Coat Biomolecular Condensates, Resembling Surfactants. To test our hypothesis, we mixed RGG-RGG (10 μM) with the amphiphilic proteins GST-GFP-RGG or MBP-GFP-RGG (1 μM) in physiological buffer and used microscopy to observe the resulting assemblies. In these systems, RGG-RGG phase separated into spherical protein droplets, as expected. Remarkably, MBP-GFP-RGG formed green rings around the RGG-RGG condensates, as observed by confocal fluorescence microscopy (Fig. 1*C*). Similarly, GST-GFP-RGG mixed with RGG-RGG formed green rings around the RGG-RGG condensates. We analyzed fluorescence intensity line profiles drawn radially across condensates in the confocal images, showing localization of GFP mainly at the condensate surface, as opposed to within or outside the condensates (Fig. 1*C*). Quantification of the partitioning of both surfactant-like proteins indicates a subtle difference. While GST-GFP-RGG localized almost entirely to the interface, MBP-GFP-RGG exhibits an elevated concentration in the dilute phase (ratio of concentrations at interface: condensate: buffer for GST-GFP-RGG is 1: 0.05: 0.01 and for MBP-GFP-RGG is 1: 0.05: 0.3). This might suggest a higher affinity between the GST-GFP-RGG protein and RGG-RGG condensate when compared to MBP-GFP-RGG. In both cases, these data demonstrate that the amphiphilic proteins adsorb to and form a layer at the condensate surface, reminiscent of surfactant-stabilized emulsions. This

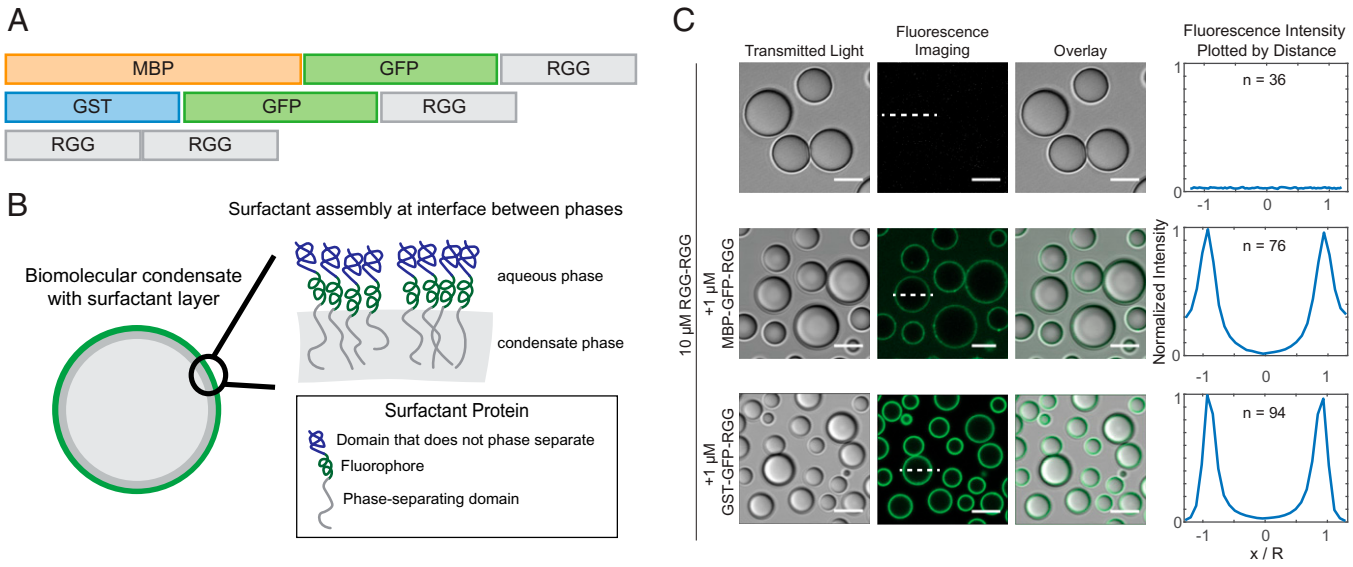

Fig. 1. Amphiphilic proteins MBP-GFP-RGG and GST-GFP-RGG form a film around RGG-RGG. (*A*) Schematic domain diagram for MBP-GFP-RGG, GST-GFP-RGG, and RGG-RGG. Length is proportional to number of residues. (*B*) Schematic model of the interaction between amphiphilic proteins and RGG-RGG. The amphiphilic protein is depicted at the interface between the two phases, surrounding the RGG-RGG core, with the phase-separating RGG domain facing the RGG-RGG core and the non–phase-separating GST or MBP domain facing the aqueous phase. (*C*) Transmitted light and fluorescence-imaging of the film formed by mixing RGG-RGG and MBP-GFP-RGG or GST-GFP-RGG in a 10:1 concentration ratio (10 μM RGG-RGG and 1 μM MBP-GFP-RGG or GST-GFP-RGG). For this and subsequent figures, buffer was 150 mM NaCl and 20 mM Tris, pH 7.5, unless stated otherwise. (*Right*) Fluorescence intensities were quantified as line profiles across individual condensates, which were normalized and averaged. *n*, number of condensates. (Scale bars, 5 μm.)

surfactant-like assembly was observed even upon shuffling the sequence of the RGG domains used to form the droplet core, suggesting that the adsorption does not depend on the precise sequence of the phase-separating IDP (*SI Appendix*, Fig. S2).

To confirm the mechanism by which the amphiphilic proteins adsorb to the interface, we examined how the fluorescence localization changes when the RGG-phillic and RGG-phobic regions of the amphiphilic protein are uncoupled. We therefore included a tobacco etch virus (TEV) protease recognition site immediately N-terminal to the RGG domain of MBP-GFP-RGG so that upon treatment with TEV protease, MBP-GFP would be liberated from RGG (Fig. 2*A*). We hypothesized that when TEV protease is added to RGG-RGG condensates enveloped by an MBP-GFP-RGG film, the cleaved RGG domain from the surfactant protein would partition into the RGG-RGG condensates, whereas the MBP-GFP would partition into the surrounding dilute phase, so the fluorescence intensity of the ring would decrease (Fig. 2*B*). Indeed, using time-lapse confocal microscopy, we observed the intensity of the fluorescent ring rapidly diminish following TEV protease addition (Fig. 2 *C* and *D*). The fluorescence intensity of the rings, f(t), decays approximately exponentially with time. The data are consistent with first-order kinetics, $f(t) = a * e^{-k*t}$, which is expected for an enzyme-catalyzed reaction in which the enzyme is not saturated by the substrate ([GST-GFP-RGG] of 1 μM ≪ Michaelis constant K_m of TEV protease, ~61 μM) (41). As a control, we performed the same experiment without TEV protease to account for photobleaching and observed only slow, linear decrease in fluorescence intensity (*SI Appendix*, Fig. S3). Collectively, these results support the model that MBP-GFP-RGG and related proteins localize to the condensate interface due to their amphiphilic nature.

Surfactant-Like Proteins Influence Condensate Size. In conducting the aforementioned TEV protease experiments, we observed that removing the protein film from around the RGG-RGG condensates triggered droplet fusion events. We sought to further understand this result, asking whether the amphiphilic proteins can influence condensate size by acting as biological surfactants and stabilizing condensates against fusion. We therefore measured droplet sizes upon mixing RGG-RGG with various concentrations of the amphiphilic protein MBP-GFP-RGG (Fig. 3*A*). As the concentration of MBP-GFP-RGG increased, the droplet sizes decreased significantly, as observed by brightfield and confocal microscopy (Fig. 3*B*). This would be expected for surfactants in a surfactant-poor regime, in which there is no excess of emulsifier (42). Since the condensates displayed a wide range of sizes for any given MBP-GFP-RGG surfactant concentration, we plotted histograms of droplet size, further revealing a shift from larger condensates in the absence of surfactant to numerous smaller condensates as surfactant concentration increases (Fig. 3*C* and *SI Appendix*, Fig. S4*A*) (interestingly, size distribution consistently appeared bimodal in several conditions, which is reminiscent of observations in nanocrystal growth in which the smaller-size mode corresponds to primary nucleation and the larger-size mode to the nanocrystals growing by aggregation) (43). Total condensate volume is approximately conserved (±19%) across samples with differing surfactant concentrations, supporting the theory that surfactant proteins do not inhibit phase separation but rather stabilize droplet size. Motivated by studies on synthetic triblock polymer surfactants comprised of a hydrophobic block sandwiched between hydrophilic blocks, we wondered how our results may differ if the RGG domain were placed as the middle block of a surfactant protein. We therefore switched the order of the fluorescent and phase-separating domains, forming MBP-RGG-GFP. We confirmed that MBP-RGG-GFP also coats RGG-RGG condensates, appearing as fluorescent rings under confocal microscopy. Similar to MBP-GFP-RGG, increasing concentrations of MBP-RGG-GFP resulted in decreased RGG-RGG droplet size (Fig. 3 *D*–*F* and *SI Appendix*, Fig. S4*B*).

Using this system, we also measured how RGG-RGG droplet size changes over time with or without MBP-RGG-GFP surfactant. Without a stabilizing mechanism and provided that droplets do not age, condensates would be expected to grow over time due to coalescence and Ostwald ripening (44).

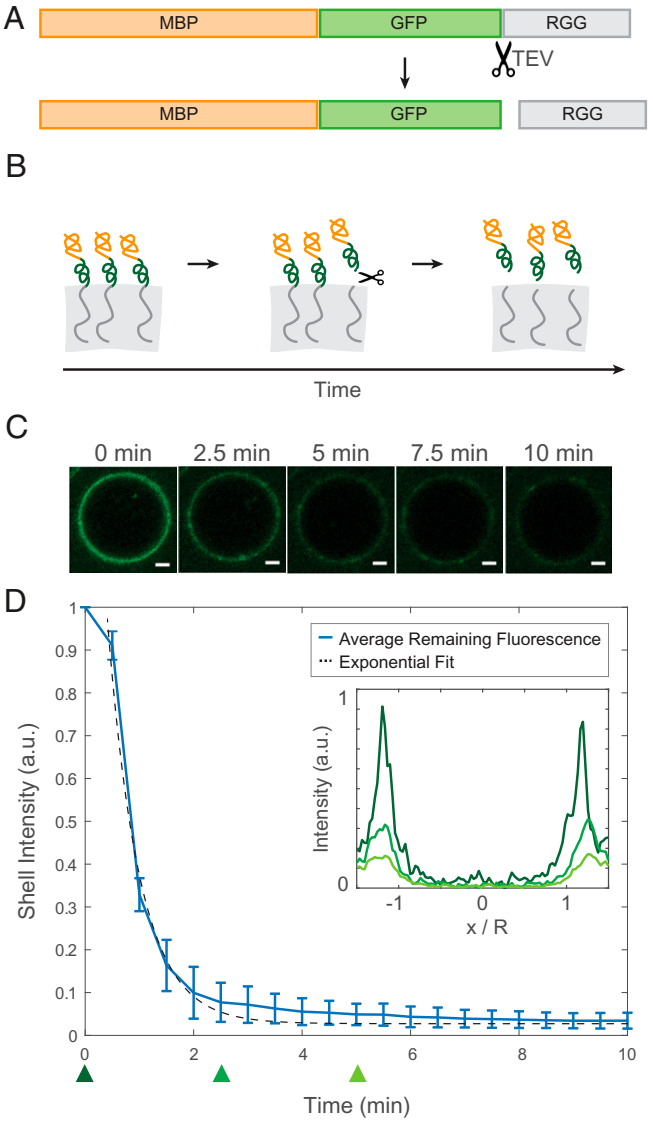

Fig. 2. Desorption of surface-associated amphiphilic protein triggered by proteolytically cleaving the dissimilar domains. (*A*) Schematic depicting the location of the TEV protease cleavage site inserted into MBP-GFP-RGG between the GFP and RGG domains. (*B*) Schematic model of the result of adding TEV protease to the RGG-RGG and MBP-GFP-RGG system. Cleavage of the amphiphilic protein results in the release of the fluorescently tagged MBP domain into the aqueous solution and retention of the RGG domain by the condensed phase. (*C*) Representative droplet images at 0, 2.5, 5, 7.5, and 10 min after TEV protease addition. (Scale bars, 1 μm.) (*D*) Total fluorescence intensity of the shell region decreases over time with the release of MBP-GFP following cleavage of MBP-GFP-RGG by TEV protease, which was added at t = 0 (plot shows average of $n = 87$ droplets). (*Inset*) Normalized average fluorescence intensity line profiles at time 0 (dark green), 2.5 min (medium green), and 5 min (light green). DTT was added to the buffer to a final concentration of 5 mM, in accordance with recommended TEV protease protocols.

We examined droplet size at timepoints of 1, 3, 6, and 24 h, finding that without surfactant, average droplet size indeed grew significantly over time (from average radius of 3.0 μm at hour 1 to 19.0 μm at hour 24). In stark contrast, we observed only a slight size increase for the surfactant-coated condensates (from average radius of 2.3 μm at hour 1, to 3.7 and 3.3 μm at hour 24, for 1 μM and 5 μM MBP-RGG-GFP, respectively). These data illustrate the lasting stabilizing effect of the surfactant layer (Fig. 3*G* and *SI Appendix*, Fig. S4*C*).

In the aforementioned experiments, RGG-RGG and MBP-RGG-GFP were mixed at the start of the experiment so that surfactant protein was present from the onset of phase separation (*SI Appendix*, Fig. S4*C*). To further understand the mechanism of size stabilization, we next conducted an alternate experiment, in which RGG-RGG condensates were allowed to grow for 1 h in the absence of surfactant, and then surfactant was added gradually in intervals (*SI Appendix*, Fig. S4*D*). In both cases, droplet sizes were smaller at 24 h compared to the negative control (i.e., RGG-RGG with no surfactant added). However, after 24 h of observation, a subset of the droplets remained larger when surfactant was added gradually compared to when surfactant was present at the onset of phase separation. This suggests that the distribution of droplet sizes may be dependent on system history. These results indicate that the surfactant proteins kinetically stabilize droplets against coarsening by coating the droplets with an amphiphilic layer. Our current data do not allow us to conclusively determine whether our RGG-RGG plus surfactant systems constitute a microemulsion, which is defined as a thermodynamically stable dispersion in which droplets can undergo both spontaneous coalescence and breakup (45).

To explore the implications of these results, we further examined how droplet size changes upon triggered removal of the surfactant layer. We added TEV protease to RGG-RGG condensates coated with MBP-x-RGG-GFP, in which x denotes a TEV protease recognition sequence, and we measured the change in cross-sectional area of the condensates over time. Here, the TEV protease cut site is placed such that MBP is liberated alone and GFP remains attached to RGG, so TEV protease treatment causes the green fluorescence to relocalize from the interface to the interior of the condensates (Fig. 3*H*). Strikingly, removal of the surfactant layer triggered rapid fusion events, leading to a significant increase in droplet size. A majority of fusion events and size increase occurred within the first 5 min after TEV protease addition (*SI Appendix*, Fig. S4*E*), after which droplet size stabilized. As a control, we added TEV protease to a sample containing only RGG-RGG. Though scattered fusion events occurred due to the creation of flow, the average droplet size did not change significantly. Overall, our results suggest that condensate size can be restricted by surfactant proteins, dependent on surfactant concentration and tunable via stimuli that manipulate the interfacial properties.

Rich Phase Behavior with Increasing Concentrations of GST-GFP-RGG. Next, we investigated the impact of altering the stoichiometry of the system. The experiments in which we varied the concentrations of MBP-GFP-RGG or MBP-RGG-GFP suggested that at high concentrations (we assessed up to 40 μM), the amphiphilic protein can accumulate in the continuous phase (Fig. 3 *B* and *E* and *SI Appendix*, Fig. S4*F*). An alternative scenario, however, is that at high concentrations, the amphiphilic protein could itself phase-separate, resulting in multiphasic behavior. A growing body of literature supports the existence and important role of multiphasic behavior in biological (13, 14, 46) and polymer-based systems (47). We therefore considered whether this occurs in our system, focusing on GST-GFP-RGG based on its lower partition coefficient in the continuous phase as compared to the MBP-based surfactants (Fig. 1*C*). For these experiments, we used buffer consisting of 150 mM NaCl and 20 mM Tris, pH 7.5, with no reducing agent added.

Remarkably, we observed rich phase behavior in a system of varying concentrations of RGG-RGG plus GST-GFP-RGG. The various assemblies can be categorized into three regimes. As described previously, at a low concentration of GST-GFP-RGG relative to RGG-RGG, we observed that RGG-RGG condensates are coated with a film of GST-GFP-RGG (Fig. 4*A*, *Left*). With increasing relative concentration of GST-GFP-RGG to RGG-RGG, a transition occurs to a second regime in which

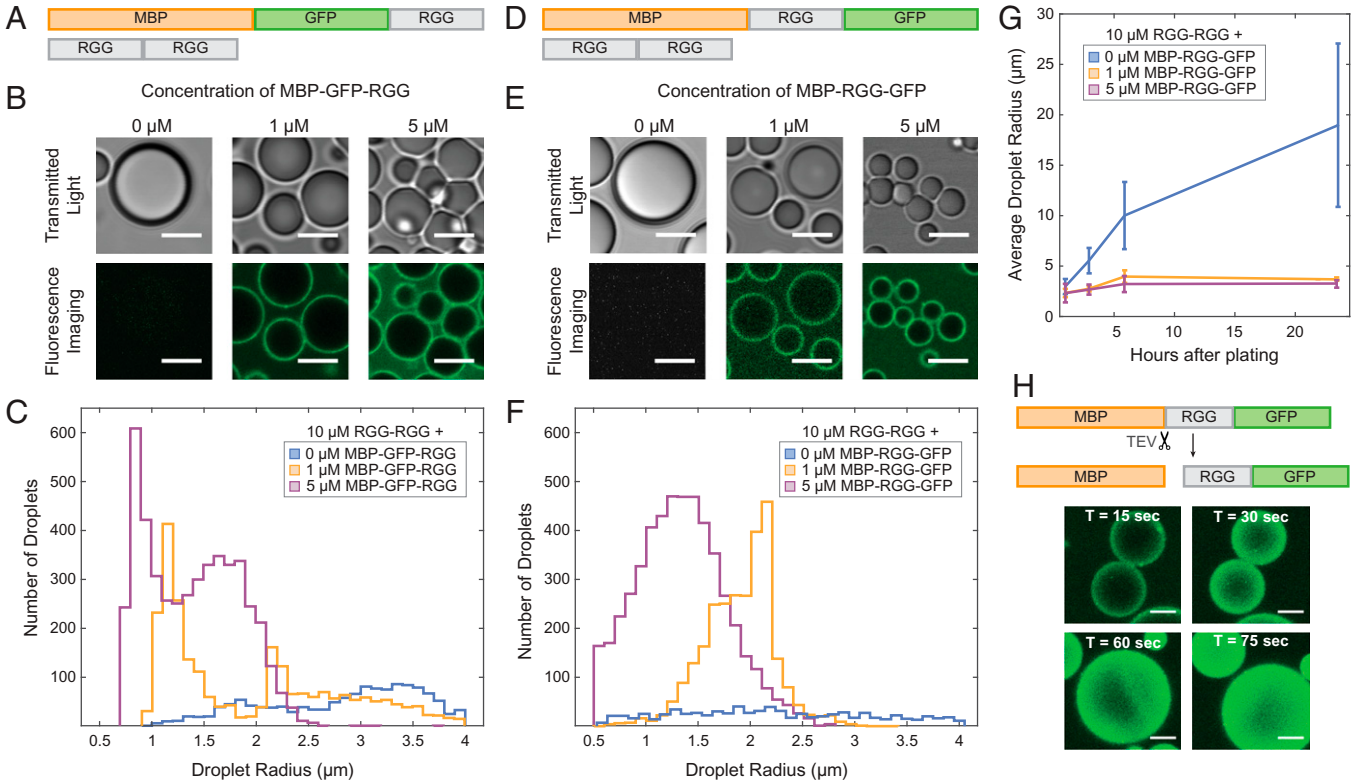

Fig. 3. Amphiphilic proteins MBP-GFP-RGG and MBP-RGG-GFP act as surfactants by stabilizing small condensates. (*A*) Domain schematics depicting surfactant protein MBP-GFP-RGG and core protein RGG-RGG. (*B*) Transmitted light and confocal fluorescence imaging of the condensates formed by mixing RGG-RGG (10 μM) with different concentrations of MBP-GFP-RGG. Droplet size becomes smaller as MBP-GFP-RGG concentration increases. (Scale bars, 5 μm.) (*C*) Histogram depicting significant shift from a small number of large condensates when no surfactant protein is added to a large number of small condensates with increasing surfactant protein concentration ($P < 0.005$ based on one-way ANOVA followed by Tukey's post hoc test). (*D*) Schematic depicting MBP-RGG-GFP and RGG-RGG. (*E*) Micrographs depict progressively smaller droplet sizes with increasing concentrations of MBP-RGG-GFP, similar to the result for MBP-GFP-RGG. (Scale bars, 5 μm.) (*F*) Histogram depicting shift in number and size of condensates with increasing concentrations of MBP-RGG-GFP ($P < 0.005$ based on one-way ANOVA followed by Tukey's post hoc test). (*G*) Surfactant stabilization of droplet size is sustained after 3, 6, and 24 h ($P < 0.05$ based on one-way ANOVA followed by Tukey's post hoc test). (*H*) TEV protease cleaves the MBP-RGG-GFP construct between MBP and RGG, releasing MBP and causing partitioning of RGG-GFP into the RGG-RGG condensates. Rapid fusion events can be observed upon disassembly of the MBP-RGG-GFP layer. (Scale bars, 1 μm.)

GST-GFP-RGG phase-separates and forms puncta that partially engulf the core droplet (Fig. 4*A*, *Middle*). Upon still further increasing the relative concentration of GST-GFP-RGG to RGG-RGG, the two proteins assemble into a multiphasic system where a continuous GST-GFP-RGG phase envelops RGG-RGG droplets (Fig. 4*A*, *Right*). The formation of a GST-GFP-RGG phase at high concentrations, whereas MBP-based amphiphiles did not display such behavior, implies a higher interaction strength between GST domains and/or between GST and the RGG-RGG core.

To further explore this range of behaviors, we mapped the phase space by varying the concentrations of both RGG-RGG and GST-GFP-RGG (Fig. 4*B*). When 1 μM GST-GFP-RGG was added to 3, 5, or 10 μM RGG-RGG, we observed films of GST-GFP-RGG coating the RGG-RGG condensates, agreeing with our prior observations. When the concentration of GST-GFP-RGG was increased to 5 μM, we observed the formation of partially engulfed RGG-RGG droplets. At a GST-GFP-RGG concentration of 10 μM, we observed partial engulfment at high RGG-RGG concentration (10 μM), shifting to multiphasic behavior at lower RGG-RGG concentration. Finally, increasing the concentration of GST-GFP-RGG further to 30 μM resulted in a greater volume of the GST-GFP-RGG phase. We can schematically summarize the phase diagram based on these qualitative categorizations for each concentration pair (Fig. 4*C*). Notably, this phase behavior remained upon imaging the samples again after 24 h (*SI Appendix*, Fig. S5).

Next, we generated three-dimensional (3D) reconstructions of condensates from confocal z-stacks to show the degree of coverage of GST-GFP-RGG surrounding the RGG-RGG phase. In the first regime, with low GST-GFP-RGG concentration, the 3D reconstruction showed a homogenous fluorescent film surrounding the RGG-RGG condensate (Fig. 4*D*, *Left*). At higher concentrations of GST-GFP-RGG, the 3D reconstructions revealed small GST-GFP-RGG condensates decorating larger RGG-RGG condensates (Fig. 4*D*, *Middle*). Still further increase of GST-GFP-RGG concentration resulted in increased surface coverage by the GST-GFP-RGG phase (Fig. 4*D*, *Right*). Next, to better visualize the multiphasic regime at relatively low RGG-RGG and high GST-GFP-RGG concentrations, we added a small amount of rhodamine B to the system (Fig. 4*E*). The rhodamine strongly partitioned into both the RGG-RGG and GST-GFP-RGG phases (partition coefficients of 21 and 17, respectively, defined as the ratio of rhodamine fluorescence in each condensate phase to that of the dilute phase). This confirms that the voids observed in the GST-GFP-RGG phase are composed of condensed RGG-RGG, rather than buffer. Finally, we tested the liquidity of the GST-GFP-RGG phase compared to the RGG-RGG phase using fluorescence recovery after photobleaching (FRAP). We observed a dramatic difference: GST-GFP-RGG exhibited slow and incomplete recovery (~10% recovery after 1 min), compared to the faster and almost complete RGG-RGG recovery (~70% after 1 min; *SI Appendix*, Fig. S6) (33, 48). This FRAP data suggests that GST-

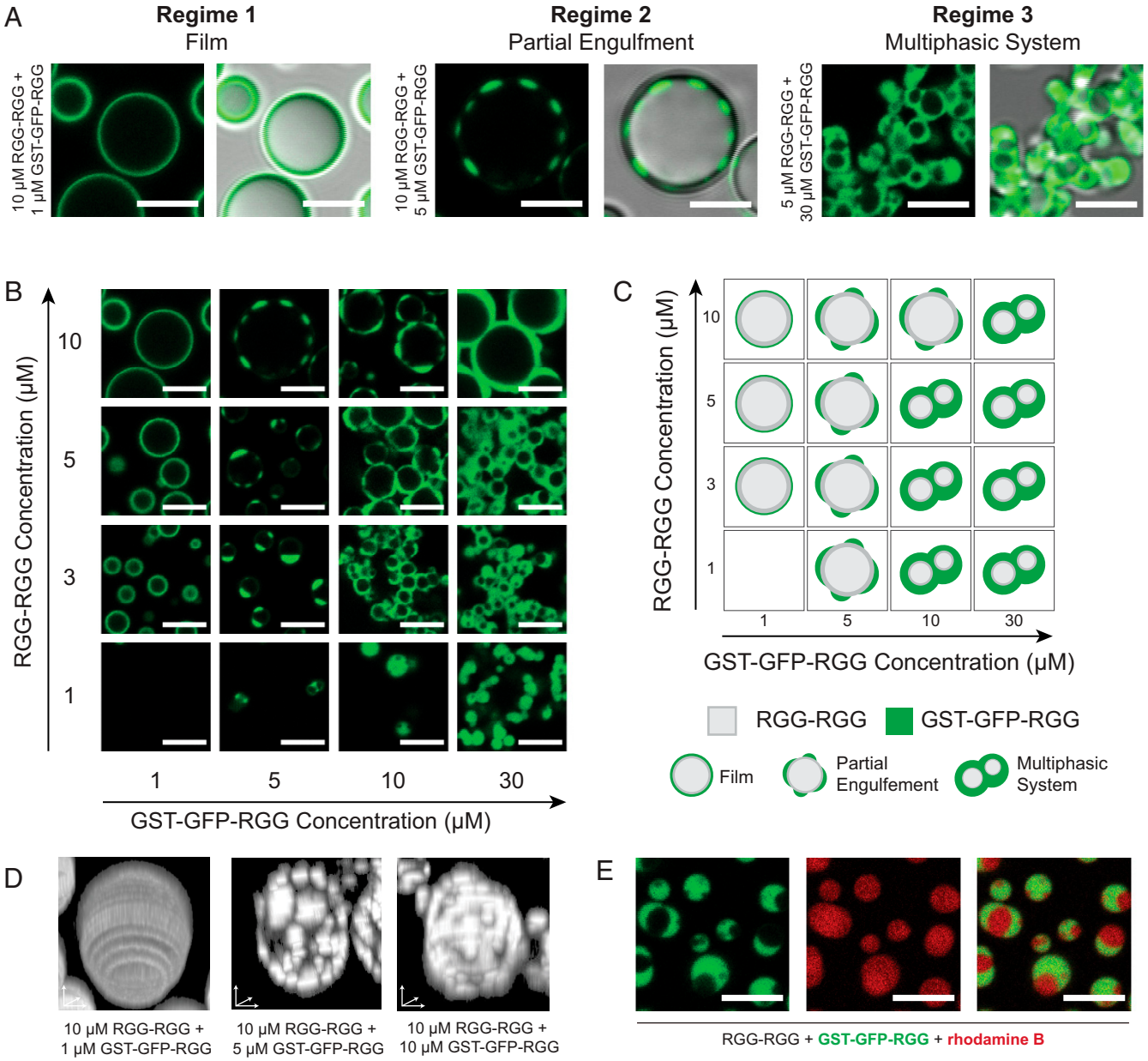

Fig. 4. Rich phase behavior of the system depends on stoichiometry of RGG-RGG and GST-GFP-RGG. (*A*) Classification system for the morphologies formed by mixing different ratios of RGG-RGG to GST-GFP-RGG. (*B*) Representative images of condensates formed across concentrations of RGG-RGG and GST-GFP-RGG tested, depicting a range of phase behaviors. (*C*) Application of classification system to the assemblies observed in the phase diagram, including film, partial engulfment, and multiphasic complexes. (*D*) Representative condensates viewed with 3D renderings depicting (*Left*) film, (*Middle*) low-coverage partial engulfment, and (*Right*) high-coverage partial engulfment. (*E*) Dual-color imaging of multiphasic system incorporating rhodamine B to confirm presence of RGG-RGG in engulfed phase. (Scale bars, 5 μm.)

GFP-RGG has a significantly higher viscosity compared to RGG-RGG.

GST-Based Surfactants Outcompete MBP-Based Surfactants at Binding to the Condensate Interface. At first glance, GST-based and MBP-based amphiphiles exhibit similar behavior when either of the amphiphilic proteins is mixed at low concentration (1 μM) with RGG-RGG (10 μM), forming core condensates enveloped by thin surfactant films. However, we previously noted subtle differences in partitioning of GST-GFP-RGG versus MBP-GFP-RGG in this regime. Whereas GST-GFP-RGG was highly localized to the droplet surface, MBP-GFP-RGG was somewhat less so, with measurable MBP-GFP-RGG fluorescence in the continuous phase (*SI Appendix*, Fig. S4*F*). This notion is further supported by the differing behaviors of these proteins at increased concentrations, wherein GST-GFP-RGG phase-separates preferentially at the RGG-RGG droplet surface, while excess MBP-GFP-RGG accumulates in the continuous phase. This raises the question of how GST-based and MBP-based surfactants would behave upon mixing RGG-RGG concurrently with both GST-based and MBP-based surfactants. Based on our prior observations, we hypothesized that the two amphiphiles may compete for binding to the interface.

To begin, we needed to examine the effects on biomolecular assembly of varying the fluorescent protein. Both the GST-based and MBP-based surfactants displayed consistent behavior

when GFP was replaced with the monomeric RFP mCherry (Fig. 5*A*). Irrespective of fluorophore, the amphiphilic proteins (1 μM) individually colocalized to the surface of RGG-RGG (10 μM) droplets. This allowed us to assess interactions between the amphiphilic proteins, focusing on the role of GST versus MBP, regardless of the fluorophore.

In agreement with our hypothesis, when we mixed the two classes of surfactant proteins together with RGG-RGG, GST-based proteins displaced MBP-based proteins from the condensate interface (Fig. 5*B*). When GST-mCherry-RGG and MBP-GFP-RGG together were mixed with RGG-RGG, we observed red rings of GST-mCherry-RGG surrounding RGG-RGG droplets, while MBP-GFP-RGG appeared mostly in the continuous phase. Likewise, when GST-GFP-RGG was mixed with MBP-mCherry-RGG, green rings of GST-GFP-RGG formed while red fluorescence was distributed throughout the continuous phase, indicating that MBP-mCherry-RGG was displaced from the interface. Plotting intensity versus radial distance confirmed that proteins with a GST tag remained adsorbed to the surface, whereas MBP-tagged proteins were displaced, irrespective of the fluorescent tag used. As a control, we sought to further verify that the choice of fluorophore has negligible impact on amphiphilic protein adsorption to the RGG-RGG surface (Fig. 5*C*). We mixed RGG-RGG, GST-GFP-RGG, and GST-mCherry-RGG. Separately, we mixed RGG-RGG plus the two MBP-based proteins with differing fluorophores. In both cases, we observed colocalized fluorescent rings in the mCherry and GFP channels via confocal microscopy, resulting in yellow rings in the merged-channel view. This suggests that amphiphiles with the same RGG-phobic domain do not displace each other and are therefore likely to have similar binding affinities to the interface.

Finally, we asked whether this competition phenomenon is concentration dependent. To test this, we prepared RGG-RGG (10 μM) plus MBP-mCherry-RGG (1 μM) with varying GST-GFP-RGG concentrations (*SI Appendix*, Fig. S7*A*). Interestingly, with only 0.1 μM GST-GFP-RGG, MBP-mCherry-RGG remained enriched at the RGG-RGG interface. As we increased the concentration of GST-GFP-RGG to 0.5 μM and higher, it out-competed MBP-mCherry-RGG for binding, causing decreased red fluorescence at the droplet surface. Quantification of the fluorescence intensity of the films formed shows that GST-GFP-RGG saturates the surface of the RGG-RGG droplets at concentrations above 0.5 μM (*SI Appendix*, Fig. S7*B*). These results suggest that GST-based surfactant proteins displace MBP-based surfactant proteins through competitive binding at the interface. This phenomenon may be due to higher solubility of the MBP tag relative to the GST tag. The higher solubility of MBP-based proteins can also be observed in the sample containing MBP-mCherry-RGG and MBP-GFP-RGG, in which the continuous phase is more fluorescent as compared to the system containing GST-mCherry-RGG and GST-GFP-RGG (Fig. 5*C*). The strong interactions between the GST domains suggested by their multiphasic behavior (Fig. 4) may also be contributing to localizing the GST-based constructs at the interface.

Domain Interactions Determine Behavior of Amphiphilic Proteins. We aimed to synthesize a mechanistic explanation for the divergent behaviors that we observed with MBP- and GST-based amphiphilic proteins. To summarize these behaviors, GST-based amphiphiles display low partitioning in solution and phase-separate at concentrations at or above ∼5 μM. MBP-based amphiphiles are relatively more available in solution and do not phase-separate at high concentrations, rather influencing condensate size. When mixed together, GST-based amphiphiles outcompete MBP-based amphiphiles for the surface of RGG-RGG condensates. Our analyses also rule out that the fluorophore has a significant impact on amphiphile behavior, indicating that properties intrinsic to GST and MBP are critical. We hypothesized that the relative strengths of interactions between domains determine both the degree of partitioning of the amphiphile to the surface as well as the formation of hierarchical structures. To account for the behaviors observed, we must consider homotypic interactions (MBP:MBP, GST:GST, and RGG:RGG) and heterotypic interactions between amphiphilic proteins and the RGG-RGG core. As mentioned earlier, strong interactions between either GST:RGG or GST:GST could be driving the formation of the multiphasic systems observed.

To explore the role of protein interactions further, we built a computational model that could recapitulate our experimental observations and provide insight into the role of interactions in determining amphiphilic protein behavior. We represented proteins as diblock copolymers, in which each domain (block) is comprised of 20 beads on a chain, with identical bonds connecting monomers and domains. This highly simplified model allowed us to simulate multicomponent phase separation using molecular dynamics (MD) simulations. The computational efficiency of the model allows us to scan a wide parameter space of interdomain interactions and protein concentrations. Based on our experimental observations, two assumptions were made: 1) the fluorescent tag does not play a major role in dictating the observed behavior and hence can be excluded from this simplified model, and 2) among all interactions possible, homotypic interactions between RGG domains are the strongest, supported by its high propensity to phase separate. All other heterotypic and homotypic interaction strengths in the system are scaled with respect to the strength of homotypic RGG interaction.

We first examined a two-component system with RGG-RGG and either MBP-RGG or GST-RGG. While presenting results from MD simulations of this two-component system, we refer to the MBP/GST domains as "X" and the RGG domain as "A." To decide on a suitable range for heterotypic interaction strength (ε_{XA}) and homotypic interaction strength (ε_{XX}), we spanned the parameter space, searching for results that approximated our experimental observations. To do so, we calculated the dilute, interfacial, and dense phase concentrations of the molecules across a range of interaction strengths and found those values at which molecules are enriched in a similar pattern as observed in our experiments (*SI Appendix*, Fig. S8). Our aim was to identify interaction criteria in which GST-RGG and MBP-RGG form a film surrounding RGG-RGG, and upon increasing the concentration of GST-RGG, we observe phase separation, whereas upon increasing the concentration of MBP-RGG, we observe accumulation in the dilute phase.

Results from the simulations can be categorized into three different regimes across the homotypic (ε_{XX}) and heterotypic (ε_{XA}) interaction space (*SI Appendix*, Fig. S9*A*), with each regime varying in terms of the distribution of the X-A chains in the system. At low homotypic and heterotypic interaction strengths, we observe that X-A chains are adsorbed to the surface of the A-A condensate, driven by A:A interactions between the A domains in A-A chains and the A domain in the X-A chains. We define this interaction parameter space as regime I, with negligible concentration of X-A in the core, a relatively higher concentration of X-A at the periphery of the A-A condensate, and with a dilute phase concentration of X-A equivalent to its solution concentration, indicating no phase separation of the X-A chains (*SI Appendix*, Fig. S9*B*, *Left*). From the experimental studies discussed earlier, MBP-RGG behavior appears to be similar to what we observe for interaction parameters in regime I. As we increase the homotypic (ε_{XX}) and heterotypic (ε_{XA}) interaction strengths further, we observe an increase in the X domain concentration at the periphery of the A-A condensed phase and a decrease in its

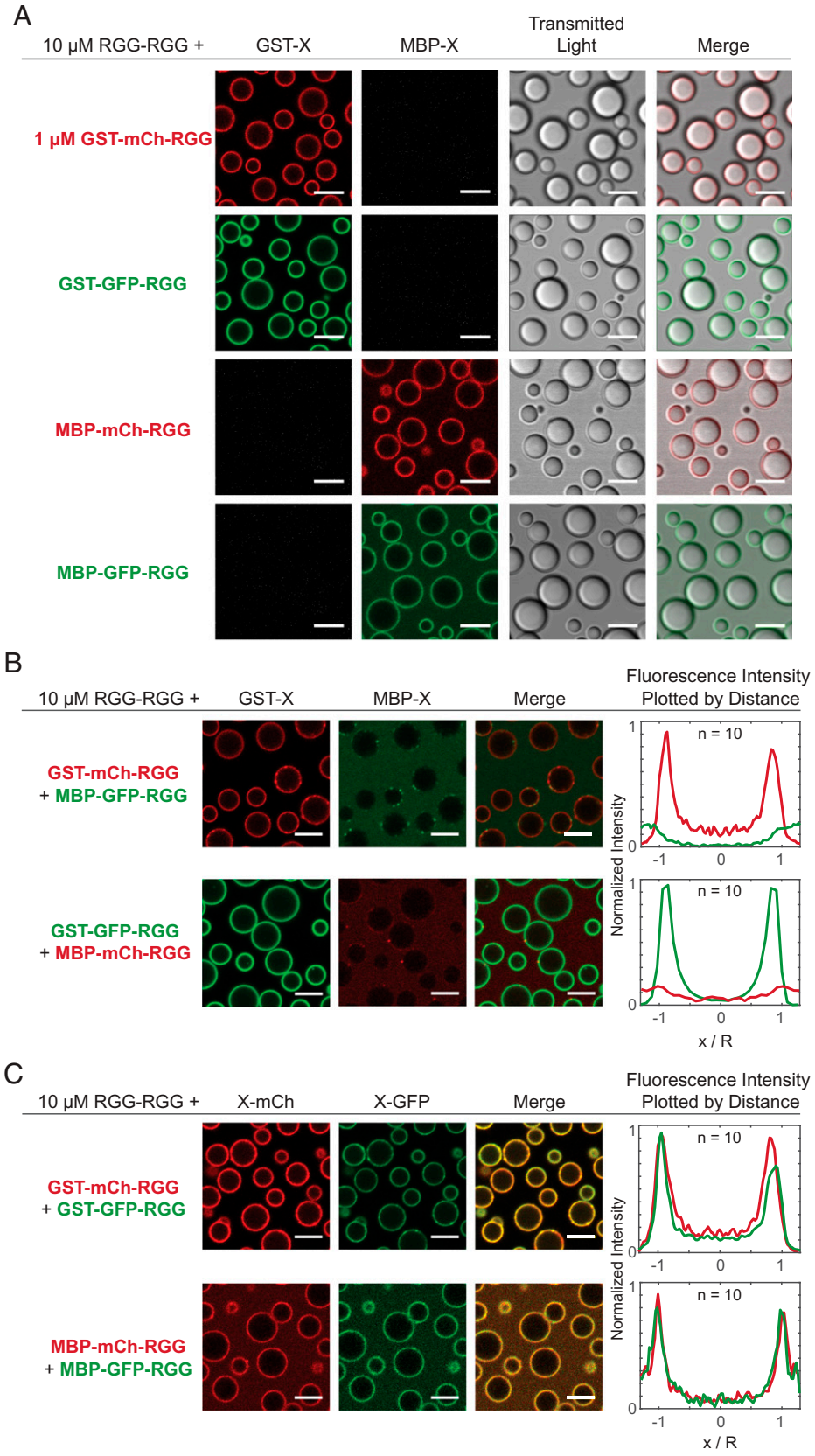

Fig. 5. Competitive adsorption to the surface of RGG-RGG condensates when two amphiphilic proteins are introduced. (*A*) Films form when a single amphiphilic protein (1 μM) is mixed with RGG-RGG (10 μM), independent of soluble domain (GST or MBP) and fluorophore (mCherry or GFP) combination used. (*B*) Combining two dissimilar amphiphilic proteins with RGG-RGG revealed competitive adsorption. Proteins with a GST domain adsorb to the RGG-RGG droplet surface, irrespective of fluorophore included. Amphiphilic proteins with an MBP domain do not adsorb to the surface. Fluorescence intensity line profiles quantified across single condensates confirm GST-containing proteins preferentially adsorb to the surface of the RGG-RGG condensates. n, number of condensates. (*C*) Simultaneous adsorption, rather than competition, is observed when combining RGG-RGG with two similar amphiphilic proteins with the same soluble domain (GST or MBP) but different fluorophores. (Scale bars, 5 μm.) Fluorescence intensity line profiles quantified across single condensates confirm simultaneous adsorption. n, number of condensates.

dilute phase concentration (*SI Appendix*, Fig. S9*B*, *Middle*). The concentration of the X domain at the core of the condensate remains negligible compared to its maximum concentration at the interface. We identify this interaction parameter space as regime II. The behavior observed in this regime relates closely to what is seen in experimental studies with RGG-RGG + ≥5 μM GST-RGG. Upon increasing the heterotypic interaction strength (ε_{XA}) even further, we shift to regime III, in which we

observe more of the X domain and hence the X-A chains within the condensed phase (*SI Appendix*, Fig. S9*B*, *Right*). This deviates from any experimentally observed behavior and implies that if RGG:GST or RGG:MBP interaction strengths were high, we would observe partitioning of GST-RGG and MBP-RGG in the RGG-RGG condensates. Further details showing the behaviors that can be observed as we vary the interaction strengths across the entire range are shown in *SI Appendix*, Fig. S10.

Next, we examined a three-component system with RGG-RGG, GST-RGG, and MBP-RGG. Within the parameter space explored, we were able to identify values for the strength of RGG:GST, RGG:MBP, GST:GST, and MBP:MBP interactions at which the model agrees with our experimental data. We set the GST:GST interaction strength to be greater than or equal to 0.8 times the RGG:RGG interaction strength (Regime II, *SI Appendix*, Fig. S9*A*) and the MBP:MBP interaction strength to be less than or equal to 0.2 times the RGG:RGG interaction strength (Regime I, *SI Appendix*, Fig. S9*A*). Results show RGG-RGG phase-separating into droplets (Fig. 6*A*, *Left*) and GST-RGG becoming highly enriched at the droplet surface (Fig. 6*A*, *Middle*), while MBP-RGG displays a weaker localization to the interface (Fig. 6*A*, *Right*). Their simulated behaviors in the dilute phase also agree with that observed experimentally, with GST-RGG being relatively more enriched at the RGG-RGG interface compared to MBP-RGG that is more present in the surrounding solution (Fig. 6*B*). We can also quantify the distribution of each component relative to the component's overall concentration (Fig. 6*C*). RGG-RGG becomes 100 times more concentrated as it phase-separates into condensates centralized at $r = 0$. GST-RGG is highly enriched (~20×) at the interface of RGG-RGG droplets at around $r = 7$ nm, thus reducing its relative concentration outside the droplet. In comparison, although we still observe some localization of MBP-RGG at the interface, it mostly remains in the surrounding solution.

To build on these observations, we explored whether the interaction values examined in the prior simulation could also produce the multiphasic behavior observed with GST-GFP-RGG. We performed a simulation of a binary mixture of RGG-RGG and GST-RGG, with GST-RGG concentration five times higher than used previously. Remarkably, the model predicts GST-RGG phase separation, represented by a dense layer of GST-RGG surrounding the RGG-RGG core. In some scenarios, multiple RGG-RGG cores can be observed within a GST-RGG phase, similar to the experimental observation of a multiphasic system (Fig. 6*D*). A reasonable explanation for this behavior is that by splitting the RGG-RGG droplet into smaller clusters, there is an increase in surface area for GST-RGG to interact with RGG-RGG molecules. Furthermore, these results support that strong homotypic interactions between GST domains drive the propensity of GST-based amphiphiles to be highly enriched at the condensate surface and to phase-separate at higher concentrations.

The simulation results for MBP-RGG are consistent with our experimental data, showing that MBP-RGG has weaker interfacial localization than GST-RGG and does not phase-separate at the conditions tested. Nonetheless, we note that our simple model cannot account for mechanisms that involve the folded structure of MBP. Experimental studies indicate that MBP enhances the solubility of its fusion partners by acting as a holdase chaperone, interacting transiently with its fusion partners to prevent their self-association (49, 50). The ligand-binding cleft in MBP appears to be important for this holdase activity (49). Future experimental studies could investigate this mechanism by testing MBP-RGG fusions with mutations that close the MBP-binding cleft (49).

Selective Tuning of Hierarchical Condensates by Modulating GST Interactions. The simulations indicated that GST-based amphiphiles phase-separate due to strong homotypic interactions between GST domains in addition to RGG:RGG interactions. Motivated by the simulations, we next sought to experimentally tease apart these interactions (Fig. 6*E*). GST-GFP-RGG at 25 μM in 150 mM NaCl buffer forms demixed condensates, but in 1 M NaCl, the GST-GFP-RGG is well mixed. This suggests that GST-GFP-RGG is indeed phase-separating due to labile intermolecular interactions, including electrostatic interactions. Next, we focused on the role of the RGG domain. Previous studies have highlighted the important role of Arg, especially Arg–Tyr interactions, in driving phase separation of RGG domains; addition of L-Arg to the buffer can interfere with these interactions and dissolve condensates (35, 51, 52). We therefore added L-Arg (100 mM) to GST-GFP-RGG, and as hypothesized, we observed that the L-Arg disrupted condensate formation. This result suggests that as expected, RGG:RGG interactions are required for GST-GFP-RGG phase separation.

However, the simulations and comparison to MBP-based amphiphiles also highlighted the important role of GST:GST interactions. Based on this information, we explored potential drivers of strong GST:GST interaction. It is known that GST has a tendency to dimerize, with a dissociation constant K_d of ~1 μM, above which dimerization is preferred (53, 54). Furthermore, GST may also oligomerize due to four cysteine residues near the protein's surface, three of which are highly solvent exposed (55, 56). We hypothesized that disulfide bonds could contribute to the tendency of GST-GFP-RGG to phase-separate (57, 58). To test this hypothesis, we assessed the impact of adding a reducing agent, which would disrupt the disulfide bonds between GST domains but which is not expected to alter the folded structure or dimerization of GST (53, 56). The experiments with GST-GFP-RGG described previously were conducted in the absence of reducing agent. Now, upon adding dithiothreitol (DTT) to GST-GFP-RGG, we observed that the condensates dissolved (Fig. 6*E*). Together, these results suggest that both RGG:RGG and GST:GST interactions are necessary for GST-GFP-RGG phase separation. The RGG domain alone has a high saturation concentration (C_{sat}) of ~50 μM in physiological buffer (35). We hypothesize that in the absence of DTT, disulfide bonds form between the GST domains and give rise to oligomers that increase the effective valency of the RGG domains, thereby promoting phase separation and reducing the C_{sat} of GST-GFP-RGG. This oligomerization may also be responsible for the slow FRAP recovery observed for GST-GFP-RGG (*SI Appendix*, Fig. S6).

We can leverage these mechanistic insights to selectively tune hierarchical condensates. RGG-RGG and GST-GFP-RGG at suitable concentrations form multiphasic condensates in 150 mM NaCl buffer, as previously described (Fig. 4). Neither RGG-RGG nor GST-GFP-RGG condensates are observed when these two proteins are prepared in 1 M NaCl buffer; rather, they are uniformly mixed in solution, because assembly of both proteins is salt sensitive (Fig. 6*F*). In contrast, upon changing the redox environment, we observed differential effects on the two phases. We examined positions in phase space in which GST-GFP-RGG and RGG-RGG form partially engulfed or multiphasic condensates in the absence of reducing agent (Fig. 6*G* and *SI Appendix*, Fig. S11). Upon adding DTT to these systems, the RGG-RGG phase remained, while the redox-sensitive GST-GFP-RGG protein no longer phase-separated. Notably, we observed a homogenous film of GST-GFP-RGG surrounding the RGG-RGG core as well as increased partitioning into the RGG-RGG phase, irrespective of the concentration of GST-GFP-RGG used. The reducing agent did not alter the RGG-RGG phase, as expected, since the RGG domain is devoid of cysteines. The transition from

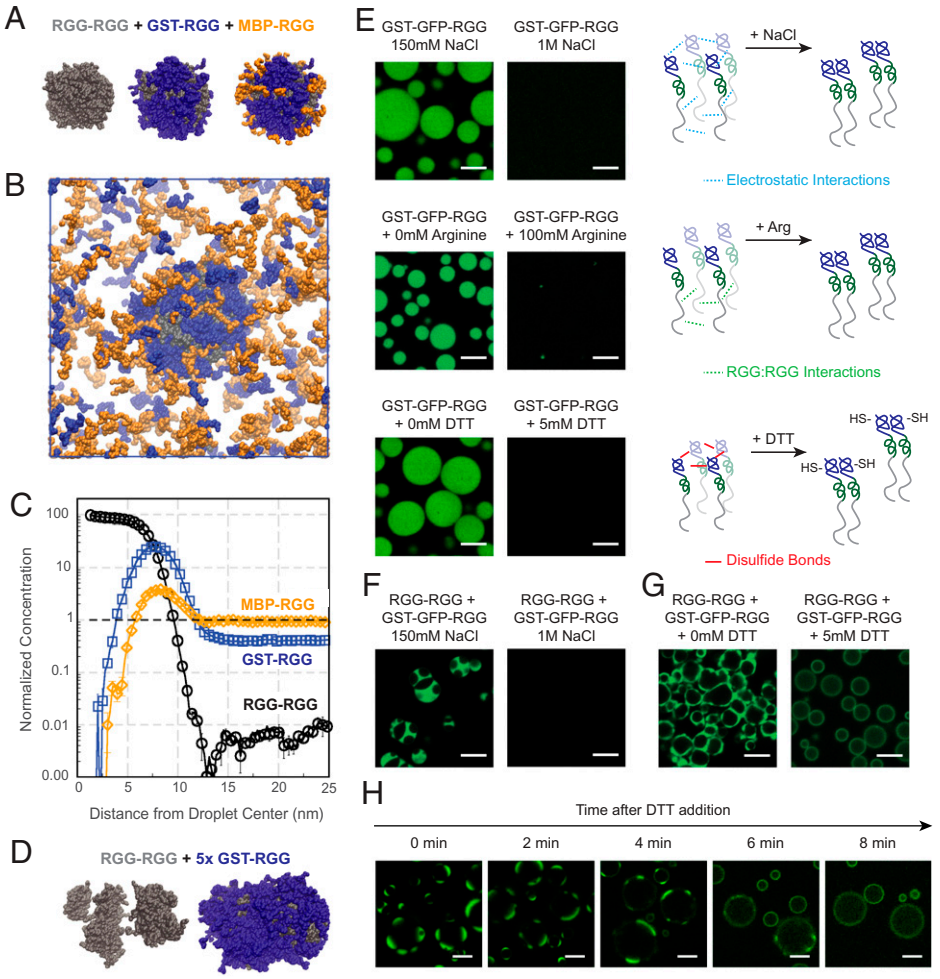

Fig. 6. Simulations identify domain interactions that can be modulated to tune multiphasic assembly. (*A*) Simulation snapshots of a condensate formed from a ternary mixture with equal concentrations of RGG-RGG (gray), GST-RGG (blue), and MBP-RGG (orange). All images are from the same snapshot, highlighting surface concentrations of different sets of components. GST-RGG displays a higher degree of coverage of the RGG-RGG surface compared to MBP-RGG. (*B*) Simulation snapshot displaying the condensed and dilute phases from *A*. Higher concentration of MBP-RGG relative to GST-RGG is observed in the dilute phase. (*C*) Quantification of protein concentration distribution in space. Protein concentration is normalized to the total concentration of each species in the solution. Mixing MBP-RGG and GST-RGG with RGG-RGG results in greater GST-RGG localization to the surface while MBP-RGG remains in solution. (*D*) MD simulation of RGG-RGG with 5× GST-RGG concentration. RGG-RGG forms multiple cores (*Left*) surrounded by a GST-RGG phase (*Right*). (*E*) Confocal fluorescence imaging of GST-GFP-RGG (25 μM) at the standard buffer conditions (150 mM NaCl and 20 mM Tris, pH 7.5) versus with 1 M NaCl (*Top*), 100 mM L-arginine (*Middle*), and 5 mM DTT (*Bottom*). Schematics illustrate that high salt hinders phase separation of GST-GFP-RGG through weakening electrostatic interactions. Addition of L-arginine prevents phase separation of GST-GFP-RGG by competing with Arg–Tyr interactions in the RGG domains, thus decreasing RGG–RGG interactions. DTT inhibits phase separation by preventing disulfide bond formation between cysteines in the GST domains. (*F*) Confocal fluorescence imaging of RGG-RGG (5 μM) and GST-GFP-RGG (10 μM) at 150 mM NaCl versus 1 M NaCl. High salt prevents phase separation of both the RGG-RGG core droplets and the surrounding GST-GFP-RGG phase. (*G*) Confocal fluorescence imaging of RGG-RGG (5 μM) and GST-GFP-RGG (10 μM) at 150 mM NaCl, without and with addition of 5 mM DTT. Addition of DTT disrupts the disulfide bonds between GST domains, resulting in loss of the GST-GFP-RGG phase and formation instead of GST-GFP-RGG films surrounding RGG-RGG droplets. RGG-RGG is devoid of Cys and is insensitive to DTT. (*H*) Time-lapse microscopy of RGG-RGG + GST-GFP-RGG after DTT addition shows the hierarchical structures evolving into film-enveloped condensates in the reducing environment. (Scale bars, 5 μm.)

multiphasic to film-enveloped condensates can be observed over time following addition of DTT (Fig. 6*H*). Collectively, these experiments highlight the tunability of the RGG-RGG + GST-GFP-RGG system, with changes to the redox environment selectively altering the GST-GFP-RGG phase, resulting in conversion between different types of hierarchical condensates. This data points to the possibility that in nature, cells may be able to exquisitely control surface interactions of biomolecular condensates through changes to the cellular environment or due to posttranslational modifications (46).

Discussion

In this paper, we demonstrate that surfactant-like proteins can contribute to the structure and regulation of biomolecular condensates. We report that a two-component in vitro system, consisting of a phase-separating protein and an amphiphilic protein, can reconstitute a range of condensate structures observed in nature. The amphiphilic protein is composed of a domain that is prone to phase-separate and a domain that does not phase-separate, so at suitable concentrations, it adsorbs to the surface of a phase-separated droplet, forming a film. Analogous to surfactant films that stabilize emulsified oil droplets, we discovered that surfactant proteins can stabilize the size of protein condensates. We also found that we can enzymatically disassemble the surfactant film and thereby trigger droplet fusion, demonstrating tunable control of condensate properties by enzymatic manipulation of surfactant proteins. Furthermore, by varying the concentrations of RGG-RGG and the GST-based amphiphiles, a rich phase behavior can be observed, reminiscent of the multiphase and multilayer structures exhibited by naturally occurring condensates. Our results highlight that different amphiphilic proteins can vary in their behavior, one consequence of which is competitive adsorption. Using a simplified model, we show that the strengths of interaction between protein domains determine the type of behavior the amphiphilic protein displays. Varying this interaction strength by modifying the environment (e.g., salt concentration and redox state) allows us to tune the behavior of the system. Future studies should further examine the effect on surfactant behavior of mutagenesis, choice of domains, orthogonality of the system, and domain architecture for both the core and surfactant proteins.

One outstanding question that our work helps address is how the size of biomolecular condensates is controlled (59, 60). Thermodynamics suggests that in the absence of a stabilizing mechanism, smaller droplets should fuse into a single large

condensate to reduce the interfacial area between the condensed and dilute phases, thereby minimizing the free energy of the system. However, frequently, cellular condensates coexist as small droplets that are not observed to fuse. Several explanations have been proposed and are likely at play (32, 61–63). Our work provides insight into an important alternative mechanism through which droplet size may be regulated. For certain amphiphilic proteins that we tested, presence of the adsorbed surface layer stabilized droplets against fusion. Our findings raise the possibility that cells could be leveraging surfactant-like, amphiphilic proteins to control organelle surface tension and size. Relatedly, one recent study demonstrated that P granules in *C. elegans* are Pickering emulsions, in which MEG-3 clusters adsorb to the condensate interface and act as Pickering agents to slow coarsening (63). Also, relatedly, one recent computational study demonstrated that low-valency client molecules that partition with scaffold proteins could theoretically modulate condensate size by acting as surfactants and affecting droplet surface tension (64). Further studies are needed to classify the type of emulsion observed in our system. This would confirm whether the size effects observed are solely due to kinetic stabilization or whether a thermodynamically stable microemulsion is formed (45). Both scenarios are likely biologically relevant (10, 65).

Our results also contribute to the growing body of literature on naturally occurring, multilayered condensates. The coexistence of multiple phases or other hierarchical structures has been demonstrated to play important roles in cellular function, such as in the organization of protein–RNA vesicles (66), TDP-43 droplets (67), the nucleolus (13), FMRP/CAPRIN1 droplets (46), stress granules (68), and P granules (14). These hierarchical structures have been described using various terminologies, including core-shell structures (12), liquid spherical shells (67), and Pickering emulsions (63, 69). These structures have been associated with several roles, including catalytic shells (12) and selective barriers (67). Beyond the field of LLPS of IDPs, the film morphologies we observe also resemble plasma membrane vesicles (70) as well as apolipoprotein micelles (71). Hence, multiphasic or multilayer morphologies can display a wide range of behaviors and play a variety of roles in cells. Our engineered system of two proteins is reminiscent of several of these behaviors and assemblies and can therefore be useful for understanding the principles of formation of multilayered condensates. A potential future direction is to conduct a bioinformatic search for naturally occurring intracellular proteins with amphiphilic properties and systematically test whether these proteins partition to the surface of known membraneless organelles.

Our system may also serve as a base platform for designing bio-inspired materials. Related to our work, formation of spherical micelles and other assembles have been observed with elastin-like polypeptides (72), amphiphilic polymers (73, 74), and plasma proteins forming core-shell structures at the air–water interface (75). Furthermore, there is a growing field concerned with developing condensates with controllable material properties with applications in several areas such as therapeutic delivery, metabolic engineering, cellular engineering, and chemical separations (76–79). We demonstrate that we can develop a multiphase system with controllable surface-patterning depending on the construction of a modular surfactant protein. Future investigations could aim at imparting function onto our system, such as by engineering two-step reactions.

Membrane-forming lipids are the prototypical example of biological amphiphiles and are essential for the function of membrane-bound compartments (80). However, what role do amphiphilic proteins play in the formation and function of membraneless compartments? Our work advances the concept that amphiphilic proteins may contribute to the assembly and size regulation of membraneless organelles. Simple systems comprising phase-separating and amphiphilic proteins, such as those described here, can be further leveraged as models for elucidating fundamental principles governing self-assembly of film-coated and multiphasic hierarchical condensates. This work aims to serve as a basis for investigating the potentially widespread role of amphiphilic proteins in membraneless organelle biology.

Methods

Refer to *SI Appendix* for details. All genes of interest were cloned into pET vectors in frame with C-terminal 6×-His tags. Proteins were recombinantly expressed in *Escherichia coli* and purified by affinity chromatography. Confocal and brightfield microscopy were used to measure phase behavior, FRAP, and droplet size. MD simulations were conducted to determine the molecular interactions underlying the phase behavior of the various proteins.

Data Availability. MATLAB scripts and image files for quantitative image analysis have been deposited in GitHub (https://github.com/favettabruna/Amphiphilic-protein-surfactants/). All other study data are included in the article and/or *SI Appendix*.

ACKNOWLEDGMENTS. We thank Zheng Shi, Dragomir Milovanovic, Christian Hoffmann, Julie Forman-Kay, Omar Adame-Arana, and Samuel Safran for valuable feedback. B.S.S. gratefully acknowledges Daniel Hammer and Matthew Good for guidance during early stages of this project. We also thank Xinyi Li for her assistance with protein purification. This research was supported by Rutgers University startup funds, a New Jersey Health Foundation grant, and a Research Council Award (to B.S.S.). F.M.K. is supported by NIH Grant T32 GM135141. R.M.R and J.M. are supported by NIH Grant R01 GM120537. Use of the high-performance computing capabilities of the Extreme Science and Engineering Discovery Environment, which is supported by NSF Grant TG-MCB-120014, is gratefully acknowledged.

1. E. B. Wilson, The structure of the protoplasm. *Science* **10**, 33–45 (1899).
2. S. F. Banani, H. O. Lee, A. A. Hyman, M. K. Rosen, Biomolecular condensates: Organizers of cellular biochemistry. *Nat. Rev. Mol. Cell Biol.* **18**, 285–298 (2017).
3. Y. Shin, C. P. Brangwynne, Liquid phase condensation in cell physiology and disease. *Science* **357**, eaaf4382 (2017).
4. A. S. Lyon, W. B. Peeples, M. K. Rosen, A framework for understanding the functions of biomolecular condensates across scales. *Nat. Rev. Mol. Cell Biol.* **22**, 215–235 (2021).
5. S. Alberti, D. Dormann, Liquid-liquid phase separation in disease. *Annu. Rev. Genet.* **53**, 171–194 (2019).
6. B. S. Schuster *et al.*, Biomolecular condensates: Sequence determinants of phase separation, microstructural organization, enzymatic activity, and material properties. *J. Phys. Chem. B* **125**, 3441–3451 (2021).
7. S. Hawgood, J. A. Clements, Pulmonary surfactant and its apoproteins. *J. Clin. Invest.* **86**, 1–6 (1990).
8. E. J. A. Veldhuizen, H. P. Haagsman, Role of pulmonary surfactant components in surface film formation and dynamics. *Biochim. Biophys. Acta* **1467**, 255–270 (2000).
9. A. A. Hyman, C. A. Weber, F. Jülicher, Liquid-liquid phase separation in biology. *Annu. Rev. Cell Dev. Biol.* **30**, 39–58 (2014).
10. S. Cuylen *et al.*, Ki-67 acts as a biological surfactant to disperse mitotic chromosomes. *Nature* **535**, 308–312 (2016).
11. A. Yamasaki *et al.*, Liquidity is a critical determinant for selective autophagy of protein condensates. *Mol. Cell* **77**, 1163–1175.e9 (2020).
12. L. D. Gallego *et al.*, Phase separation directs ubiquitination of gene-body nucleosomes. *Nature* **579**, 592–597 (2020).
13. M. Feric *et al.*, Coexisting liquid phases underlie nucleolar subcompartments. *Cell* **165**, 1686–1697 (2016).
14. A. Putnam, M. Cassani, J. Smith, G. Seydoux, A gel phase promotes condensation of liquid P granules in *Caenorhabditis elegans* embryos. *Nat. Struct. Mol. Biol.* **26**, 220–226 (2019).
15. S. Jain *et al.*, ATPase-modulated stress granules contain a diverse proteome and substructure. *Cell* **164**, 487–498 (2016).
16. J. Fei *et al.*, Quantitative analysis of multilayer organization of proteins and RNA in nuclear speckles at super resolution. *J. Cell Sci.* **130**, 4180–4192 (2017).
17. J. A. West *et al.*, Structural, super-resolution microscopy analysis of paraspeckle nuclear body organization. *J. Cell Biol.* **214**, 817–830 (2016).
18. S. Boeynaems *et al.*, Spontaneous driving forces give rise to protein-RNA condensates with coexisting phases and complex material properties. *Proc. Natl. Acad. Sci. U.S.A.* **116**, 7889–7898 (2019).

19. R. S. Fisher, S. Elbaum-Garfinkle, Tunable multiphase dynamics of arginine and lysine liquid condensates. *Nat. Commun.* **11**, 4628 (2020).
20. T. Kaur *et al.*, Sequence-encoded and composition-dependent protein-RNA interactions control multiphasic condensate morphologies. *Nat. Commun.* **12**, 872 (2021).
21. P. Swain, S. C. Weber, Dissecting the complexity of biomolecular condensates. *Biochem. Soc. Trans.* **48**, 2591–2602 (2020).
22. D. W. Sanders *et al.*, Competing protein-RNA interaction networks control multiphase intracellular organization. *Cell* **181**, 306–324.e28 (2020).
23. G. Wan *et al.*, Spatiotemporal regulation of liquid-like condensates in epigenetic inheritance. *Nature* **557**, 679–683 (2018).
24. J. Israelachvili, *Intermolecular and Surface Forces* (Elsevier Inc., 2011).
25. C. P. Brangwynne, Phase transitions and size scaling of membrane-less organelles. *J. Cell Biol.* **203**, 875–881 (2013).
26. I. A. Klein *et al.*, Partitioning of cancer therapeutics in nuclear condensates. *Science* **368**, 1386–1392 (2020).
27. T. J. Welsh *et al.*, Surface electrostatics govern the emulsion stability of biomolecular condensates. bioRxiv [Preprint] (2020). 10.1101/2020.04.20.047910 (Accessed 7 April 2021).
28. M. Feric, C. P. Brangwynne, A nuclear F-actin scaffold stabilizes ribonucleoprotein droplets against gravity in large cells. *Nat. Cell Biol.* **15**, 1253–1259 (2013).
29. F. G. Quiroz *et al.*, Liquid-liquid phase separation drives skin barrier formation. *Science* **367**, eaax9554 (2020).
30. W. T. Snead, T. M. Gerbich, I. Seim, Z. Hu, A. S. Gladfelter, Membrane surfaces regulate assembly of a ribonucleoprotein condensate. bioRxiv [Preprint] (2021). 10.1101/2021.04.24.441251 (Accessed 14 May 2021).
31. S. Ranganathan, E. I. Shakhnovich, Dynamic metastable long-living droplets formed by sticker-spacer proteins. *eLife* **9**, 1–25 (2020).
32. J. D. Wurtz, C. F. Lee, Chemical-reaction-controlled phase separated drops: Formation, size selection, and coarsening. *Phys. Rev. Lett.* **120**, 078102 (2018).
33. B. S. Schuster *et al.*, Controllable protein phase separation and modular recruitment to form responsive membraneless organelles. *Nat. Commun.* **9**, 2985 (2018).
34. S. Elbaum-Garfinkle *et al.*, The disordered P granule protein LAF-1 drives phase separation into droplets with tunable viscosity and dynamics. *Proc. Natl. Acad. Sci. U.S.A.* **112**, 7189–7194 (2015).
35. B. S. Schuster *et al.*, Identifying sequence perturbations to an intrinsically disordered protein that determine its phase-separation behavior. *Proc. Natl. Acad. Sci. U.S.A.* **117**, 11421–11431 (2020).
36. P. A. Chong, R. M. Vernon, J. D. Forman-Kay, RGG/RG motif regions in RNA binding and phase separation. *J. Mol. Biol.* **430**, 4650–4665 (2018).
37. D. Esposito, D. K. Chatterjee, Enhancement of soluble protein expression through the use of fusion tags. *Curr. Opin. Biotechnol.* **17**, 353–358 (2006).
38. R. B. Kapust, D. S. Waugh, *Escherichia coli* maltose-binding protein is uncommonly effective at promoting the solubility of polypeptides to which it is fused. *Protein Sci.* **8**, 1668–1674 (1999).
39. E. H. Reed, B. S. Schuster, M. C. Good, D. A. Hammer, SPLIT: Stable protein coacervation using a light induced transition. *ACS Synth. Biol.* **9**, 500–507 (2020).
40. R. M. Caldwell *et al.*, Optochemical control of protein localization and activity within cell-like compartments. *Biochemistry* **57**, 2590–2596 (2018).
41. R. B. Kapust *et al.*, Tobacco etch virus protease: Mechanism of autolysis and rational design of stable mutants with wild-type catalytic proficiency. *Protein Eng.* **14**, 993–1000 (2001).
42. S. Tcholakova, N. D. Denkov, T. Danner, Role of surfactant type and concentration for the mean drop size during emulsification in turbulent flow. *Langmuir* **20**, 7444–7458 (2004).
43. F. Wang, V. N. Richards, S. P. Shields, W. E. Buhro, Kinetics and mechanisms of aggregative nanocrystal growth. *Chem. Mater.* **26**, 5–21 (2014).
44. M. Linsenmeier, M. R. G. Kopp, S. Stavrakis, A. de Mello, P. Arosio, Analysis of biomolecular condensates and protein phase separation with microfluidic technology. *Biochim. Biophys. Acta Mol. Cell Res.* **1868**, 118823 (2021).
45. M. J. Rosen, J. T. Kunjappu, *Surfactants and Interfacial Phenomena* (John Wiley & Sons, Inc., ed. 4, 2012), pp. 350–353.
46. T. H. Kim *et al.*, Phospho-dependent phase separation of FMRP and CAPRIN1 recapitulates regulation of translation and deadenylation. *Science* **365**, 825–829 (2019).
47. T. Lu, E. Spruijt, Multiphase complex coacervate droplets. *J. Am. Chem. Soc.* **142**, 2905–2914 (2020).
48. H. Wang, F. M. Kelley, D. Milovanovic, B. S. Schuster, Z. Shi, Surface tension and viscosity of protein condensates quantified by micropipette aspiration. *Biophys. Rep.* **1**, 100011 (2021).
49. S. Nallamsetty, D. S. Waugh, Mutations that alter the equilibrium between open and closed conformations of *Escherichia coli* maltose-binding protein impede its ability to enhance the solubility of passenger proteins. *Biochem. Biophys. Res. Commun.* **364**, 639–644 (2007).
50. S. Raran-Kurussi, D. S. Waugh, The ability to enhance the solubility of its fusion partners is an intrinsic property of maltose-binding protein but their folding is either spontaneous or chaperone-mediated. *PLoS One* **7**, e49589 (2012).
51. S. Alberti *et al.*, A user's guide for phase separation assays with purified proteins. *J. Mol. Biol.* **430**, 4806–4820 (2018).
52. E. Boke *et al.*, Amyloid-like self-assembly of a cellular compartment. *Cell* **166**, 637–650 (2016).
53. M. A. McTigue, D. R. Williams, J. A. Tainer, Crystal structures of a schistosomal drug and vaccine target: Glutathione S-transferase from *Schistosoma japonica* and its complex with the leading antischistosomal drug praziquantel. *J. Mol. Biol.* **246**, 21–27 (1995).
54. Y. C. Huang, S. Misquitta, S. Y. Blond, E. Adams, R. F. Colman, Catalytically active monomer of glutathione S-transferase π and key residues involved in the electrostatic interaction between subunits. *J. Biol. Chem.* **283**, 32880–32888 (2008).
55. T. Tudyka, A. Skerra, Glutathione S-transferase can be used as a C-terminal, enzymatically active dimerization module for a recombinant protease inhibitor, and functionally secreted into the periplasm of *Escherichia coli*. *Protein Sci.* **6**, 2180–2187 (1997).
56. N. Tzvetkov, P. Breuer, R. Boteva, Cysteine-free glutathione-S-transferase as a tool for thiol-specific labeling of proteins. *Biotechniques* **40**, 145–146 (2006).
57. E. H. Reed, D. A. Hammer, Redox sensitive protein droplets from recombinant oleosin. *Soft Matter* **14**, 6506–6513 (2018).
58. S. Ambadipudi, J. Biernat, D. Riedel, E. Mandelkow, M. Zweckstetter, Liquid-liquid phase separation of the microtubule-binding repeats of the Alzheimer-related protein Tau. *Nat. Commun.* **8**, 275 (2017).
59. S. C. Weber, C. P. Brangwynne, Inverse size scaling of the nucleolus by a concentration-dependent phase transition. *Curr. Biol.* **25**, 641–646 (2015).
60. F. Dar, R. Pappu, Restricting the sizes of condensates. *eLife* **9**, 1–3 (2020).
61. C. P. Brangwynne *et al.*, Germline P granules are liquid droplets that localize by controlled dissolution/condensation. *Science* **324**, 1729–1732 (2009).
62. J. Berry, C. P. Brangwynne, M. Haataja, Physical principles of intracellular organization via active and passive phase transitions. *Rep. Prog. Phys.* **81**, 046601 (2018).
63. A. W. Folkmann, A. Putnam, C. F. Lee, G. Seydoux, Regulation of biomolecular condensates by interfacial protein clusters. *Science* **373**, 1218–1224 (2021).
64. I. Sanchez-Burgos, J. A. Joseph, R. Collepardo-Guevara, J. R. Espinosa, Size conservation emerges spontaneously in biomolecular condensates formed by scaffolds and surfactant clients. *Sci. Rep.* **11**, 15241 (2021).
65. L. Hilbert *et al.*, Transcription organizes euchromatin via microphase separation. *Nat. Commun.* **12**, 1–12 (2021).
66. I. Alshareedah, M. M. Moosa, M. Raju, D. A. Potoyan, P. R. Banerjee, Phase transition of RNA-protein complexes into ordered hollow condensates. *Proc. Natl. Acad. Sci. U.S.A.* **117**, 15650–15658 (2020).
67. H. Yu *et al.*, HSP70 chaperones RNA-free TDP-43 into anisotropic intranuclear liquid spherical shells. *Science* **371**, eabb4309 (2021).
68. A. Khong *et al.*, The stress granule transcriptome reveals principles of mRNA accumulation in stress granules. *Mol. Cell* **68**, 808–820.e5 (2017).
69. C. D. Crowe, C. D. Keating, Liquid-liquid phase separation in artificial cells. *Interface Focus* **8**, 20180032 (2018).
70. T. Baumgart *et al.*, Large-scale fluid/fluid phase separation of proteins and lipids in giant plasma membrane vesicles. *Proc. Natl. Acad. Sci. U.S.A.* **104**, 3165–3170 (2007).
71. R. W. Mahley, T. L. Innerarity, S. C. Rall Jr., K. H. Weisgraber, Plasma lipoproteins: Apolipoprotein structure and function. *J. Lipid Res.* **25**, 1277–1294 (1984).
72. J. R. Simon, N. J. Carroll, M. Rubinstein, A. Chilkoti, G. P. López, Programming molecular self-assembly of intrinsically disordered proteins containing sequences of low complexity. *Nat. Chem.* **9**, 509–515 (2017).
73. A. Ianiro *et al.*, Controlling the spatial distribution of solubilized compounds within copolymer micelles. *Langmuir* **35**, 4776–4786 (2019).
74. F. Jiménez-Ángeles *et al.*, Self-assembly of charge-containing copolymers at the liquid-liquid interface. *ACS Cent. Sci.* **5**, 688–699 (2019).
75. Z. Liao, J. W. Lampe, P. S. Ayyaswamy, D. M. Eckmann, I. J. Dmochowski, Protein assembly at the air-water interface studied by fluorescence microscopy. *Langmuir* **27**, 12775–12781 (2011).
76. M. Amiram, K. M. Luginbuhl, X. Li, M. N. Feinglos, A. Chilkoti, Injectable protease-operated depots of glucagon-like peptide-1 provide extended and tunable glucose control. *Proc. Natl. Acad. Sci. U.S.A.* **110**, 2792–2797 (2013).
77. E. M. Zhao et al., Light-based control of metabolic flux through assembly of synthetic organelles. Nat. Chem. Biol.15, 589–597 (2019).
78. S. Roberts *et al.*, Complex microparticle architectures from stimuli-responsive intrinsically disordered proteins. *Nat. Commun.* **11**, 1342 (2020).
79. M. V. Garabedian *et al.*, Designer membraneless organelles sequester native factors for control of cell behavior. *Nat. Chem. Biol.* **17**, 998–1007 (2021).
80. W. F. Zeno, K. J. Day, V. D. Gordon, J. C. Stachowiak, Principles and applications of biological membrane organization. *Annu. Rev. Biophys.* **49**, 19–39 (2020).